A LETTERS JOURNAL EXPLORING THE FRONTIERS OF PHYSICS

OFFPRINT

Transport and correlated fluctuations in the nonlinear optical response of excitons

D. ABRAMAVICIUS, L. VALKUNAS and S. MUKAMEL

EPL, **80** (2007) 17005

TAKE A LOOK AT THE NEW EPL

Europhysics Letters (EPL) has a new online home at
www.epljournal.org

Take a look for the latest journal news and information on:

- reading the latest articles, free!
- receiving free e-mail alerts
- submitting your work to EPL

www.epljournal.org

A Letters Journal Exploring the Frontiers of Physics

October 2007

EPL, **80** (2007) 17005 www.epljournal.org
doi: 10.1209/0295-5075/80/17005

Transport and correlated fluctuations in the nonlinear optical response of excitons

D. Abramavicius[1], L. Valkunas[2,3] and S. Mukamel[1]

[1] *Chemistry Department, University of California Irvine - 1102 Natural Sciences 2, Irvine, CA 92697-2025, USA*
[2] *Theoretical Physics Department, Faculty of Physics of Vilnius University - Sauletekio ave. 9, bld. 3, Vilnius, LT 10222, Lithuania*
[3] *Institute of Physics - Savanoriu 231, Vilnius, LT 02300, Lithuania*

received 26 March 2007; accepted in final form 13 August 2007
published online 7 September 2007

PACS 78.47.+p – Time-resolved optical spectroscopies and other ultrafast optical measurements in condensed matter
PACS 82.53.Kp – Coherent spectroscopy of atoms and molecules
PACS 33.70.Jg – Line and band widhs, shapes, and shifts

Abstract – Closed expressions are derived for the femtosecond four-wave mixing of excitons which include slow Gaussian diagonal fluctuations (spectral diffusion) through the cumulant expansion and incoherent exciton transport induced by fast Markovian fluctuations. The interplay of both processes in the two-dimensional photon echo is demonstrated using model calculations for a dimer.

Introduction. – Two-dimensional (2D) spectroscopy is a newly developed coherent technique that projects the third-order femtosecond four-wave mixing signals onto frequency-frequency correlation plots that carry structural and dynamical information of molecules [1–3]. Recent experimental advances in heterodyne detected 2D spectroscopy in the infrared and the visible as well as theoretical progress have made it possible to study exciton dynamics and relaxation in molecules and their complexes [4–7], protein structure fluctuations and folding [8–12], and hydrogen bonding correlations [13,14].

Third-order impulsive spectroscopy is described by the response function, $S^{(3)}(t_3, t_2, t_1)$, which relates the incoming optical electric fields to the induced polarization [15]: t_1, t_2 and t_3 are the delays between chronologically ordered pulses shown in fig. 1. The time-domain signal with the wave vector $\boldsymbol{k}_S = -\boldsymbol{k}_1 + \boldsymbol{k}_2 + \boldsymbol{k}_3$, where $\boldsymbol{k}_j$ is the wave vector of pulse j, is known as the photon echo since it involves the rephasing of the system's density matrix at $t_3 = t_1$ [16]. The 2D photon echo (2D PE) signal is given by double Fourier transform ($t_1 \to \Omega_1$ and $t_3 \to \Omega_3$, at constant t_2) of the response function, $S^{(3)}(\Omega_3, t_2, \Omega_1)$ [2].

2D PE spectra contain many types of dynamical information. Diagonal peak lineshapes along $\Omega_3 = -\Omega_1$ reveal the environment fluctuations: elliptical peak patterns reflect the interplay of homogeneous and inhomogeneous broadenings. The cross (off-diagonal) peaks probe coherences, couplings, correlations and exciton transfer dynamics. Correlated exciton dynamics and population relaxation were observed in recent experiments [5,6,9]. Bath correlations show up as elongated peaks indicating that the absorption frequency is correlated with the emission frequency. The decay of these correlations can be observed through the variation of the elliptical peaks during t_2 [9]. Coherent quantum dynamics is observed as oscillations of peak amplitudes [7].

The extraction of system parameters from the 2D data requires extensive computational effort. Two different approaches are used. The direct simulation of quantum dynamics by solving the Liouville equation (non-perturbative treatment) is the most flexible approach, however, it is numerically expensive [17] and is not considered in this letter. Some statistical properties of fluctuations can be incorporated analytically using perturbative approach at varous levels [15]. Diagonal Gaussian fluctuations with arbitrary time scale and degree of correlations can be rigorously treated via the second-order cumulant expansion [18]. Exciton population relaxation (transport) is then accounted for by invoking a Markovian approximation (bath correlation time $\tau_c \to 0$) leading to the Redfield equations [4]. The combined effect of finite bath correlation time and transport can be described by including collective bath corrdinates through the stochastic Liouville equations [19–21]. However, this is practical only when

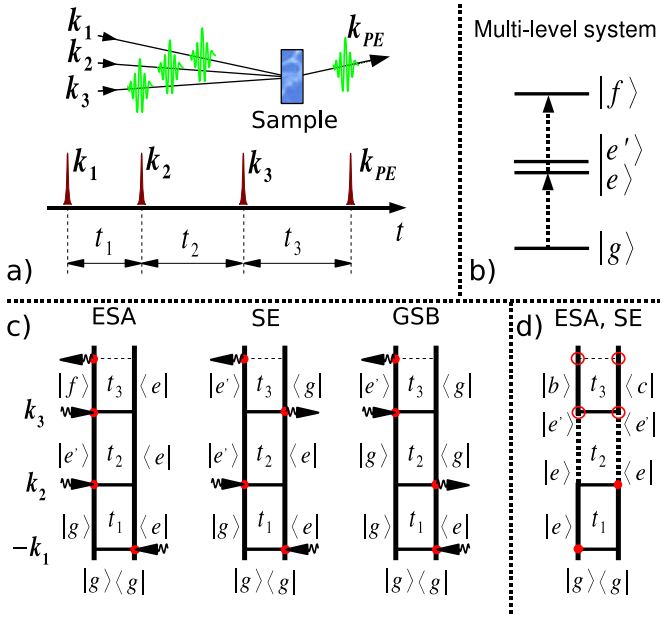

Fig. 1: (Color online) a) The 2D photon echo experiment. Three laser pulses interact with the system to generate the signal with the wave vector $\boldsymbol{k}_S = -\boldsymbol{k}_1 + \boldsymbol{k}_2 + \boldsymbol{k}_3$. t_1 and t_2 are positive delay times between pulses; t_3 is the delay between the third pulse and the detected signal. b) The energy level scheme of an excitonic system; arrows indicate resonant optical transitions. c) Feynman diagrams for the photon echo in the coherent limit. d) Population transfer diagram representing $\boldsymbol{k}_1 - \boldsymbol{k}_2 \pm \boldsymbol{k}_3$; red dots represent interactions with $\boldsymbol{k}_1$ and $\boldsymbol{k}_2$ and open circles indicate technique-dependent interactions for $\boldsymbol{k}_3$ and the signal. For photon echo the signal is then generated on the right side of the diagram: $\boldsymbol{k}_3$ interacts on the right for ESA and on the left for SE.

the number of relevant coordinates is not too large. The doorway-window representation has been used to develop approximate expressions that combine the cumulant expansion and transport in the Markovian regime ($\Lambda \gg K$; Λ^{-1} is the bath correlation timescale and K is the exciton transport rate) [4]. Extensive statistical Monte Carlo sampling (diagonal and off-diagonal disorder) is added to account for inhomogeneous broadening due to static fluctuations with long bath correlation timescales [22,23].

In this letter we generalize the doorway-window picture and develop expressions that can describe both slow bath fluctuations and transport. Two levels of theory are considered: the first includes arbitrary degree of correlation of frequency fluctuations but neglects the Stokes shift during transport, and the second is limited to correlated fluctuations but includes the Stokes shift.

Response function of excitons with diagonal fluctuations. – We consider a multilevel system described by the Hamiltonian

$$\hat{H} = \hat{H}_M - \hat{P}\cdot E, \tag{1}$$

where the system+bath Hamiltonian is

$$\hat{H}_M = \sum_\nu \varepsilon_\nu |\nu\rangle\langle\nu| + \sum_{\nu\nu'} \hat{Q}_{\nu\nu'}|\nu\rangle\langle\nu'| + \hat{H}_B. \tag{2}$$

The three terms represent, respectively, the system, the system-bath interaction and the bath. ε_ν is the energy of the eigenstate ν, $\hat{Q}_{\nu\nu'}$ is a collective harmonic bath coordinate linearly coupled to the system Hamiltonian element $|\nu\rangle\langle\nu'|$ [24] and $\hat{H}_B$ is the harmonic bath Hamiltonian.

The eigenstates of molecular aggregates typically form well-separated manifolds (see fig. 1b): $\nu = g$ with $\varepsilon_g = 0$ is the ground state, $\nu \in e$, are singly excited, while states in f, $\nu \in f$, are doubly excited. The bath induces small fluctuations to the diagonal and off-diagonal matrix elements of the system Hamiltonian. The interaction between the system and classical optical field is represented by the polarization operator

$$\hat{P} = \sum_{\nu\nu'}^{\nu\neq\nu'} \mu_{\nu\nu'}|\nu\rangle\langle\nu'| \tag{3}$$

with the transition dipole moment $\mu_{\nu\nu'}$.

The response function $S^{(3)}$ is given by the four-point correlation function of the polarization operator [15]:

$$\begin{aligned} S^{(3)}(t_3,t_2,t_1) \;=\; & i^3 F(t_1, t_1+t_2, t_1+t_2+t_3, 0) \\ & + i^3 F(0, t_1+t_2, t_1+t_2+t_3, t_1) \\ & + i^3 F(0, t_1, t_1+t_2+t_3, t_1+t_2) \\ & + i^3 F(t_1+t_2+t_3, t_1+t_2, t_1, 0) + c.c., \end{aligned} \tag{4}$$

where

$$F(\tau_4,\tau_3,\tau_2,\tau_1) = \langle \hat{P}(\tau_4)\hat{P}(\tau_3)\hat{P}(\tau_2)\hat{P}(\tau_1)\rangle \tag{5}$$

and $\hat{P}(\tau) = \exp(i\hat{H}_M\tau)\hat{P}\exp(-i\hat{H}_M\tau)$. The correlation function can be calculated exactly when off-diagonal bath fluctuations $\hat{Q}_{\nu\nu'}$ $(\nu \neq \nu')$ are neglected [18]. F can then be expanded in the system eigenstates

$$\begin{aligned} & F(\tau_4,\tau_3,\tau_2,\tau_1) = \\ & \sum_{cba} \mu_{gc}\mu_{cb}\mu_{ba}\mu_{ag}\mathcal{F}^{(C)}_{cba}(\tau_4,\tau_3,\tau_2,\tau_1), \end{aligned} \tag{6}$$

where using $\tau_{ij} = \tau_i - \tau_j$ we get:

$$\begin{aligned} \mathcal{F}^{(C)}_{cba}(\tau_4,\tau_3,\tau_2,\tau_1) \;=\; & \exp[-i(\varepsilon_c\tau_{43} + \varepsilon_b\tau_{32} + \varepsilon_a\tau_{21}) \\ & + f^{(C)}_{cba}(\tau_4,\tau_3,\tau_2,\tau_1)], \end{aligned} \tag{7}$$

and[1]

$$\begin{aligned} f^{(C)}_{cba}(\tau_4,\tau_3,\tau_2,\tau_1) = & -g_{cc}(\tau_{43}) - g_{bb}(\tau_{32}) \\ & - g_{aa}(\tau_{21}) - g_{cb}(\tau_{42}) + g_{cb}(\tau_{43}) + g_{cb}(\tau_{32}) \\ & - g_{ca}(\tau_{41}) + g_{ca}(\tau_{42}) + g_{ca}(\tau_{31}) - g_{ca}(\tau_{32}) \\ & - g_{ba}(\tau_{31}) + g_{ba}(\tau_{32}) + g_{ba}(\tau_{21}). \end{aligned} \tag{8}$$

The superscript "C" denotes the coherent (no transport) limit. The lineshape function is

$$g_{\nu\nu'}(t) = \int_0^t \mathrm{d}\tau_2 \int_0^{\tau_2} \mathrm{d}\tau_1 C_{\nu\nu'}(\tau_2 - \tau_1), \tag{9}$$

[1] Previous expressions in ref. [11] used a semiclassical approximation and the lineshape functions were therefore symmetrized with respect to ν and ν'. Here we do not invoke the semiclassical approximation.

where $C_{\nu\nu'}(\tau_2-\tau_1)\equiv\langle Q_{\nu\nu}(\tau_2-\tau_1)Q_{\nu'\nu'}(0)\rangle$ is the bath correlation function.

Response functions with exciton transport. – To include exciton population relaxation we recast the response function in the doorway-window picture [4]:

$$S^{(3)}(t_3,t_2,t_1)=-i^3\langle\langle\mathcal{W}(t_3)\mathcal{G}(t_2)\mathcal{D}(t_1)\rangle\rangle \qquad (10)$$

where $\mathcal{D}(t)\equiv\mathcal{P}\mathcal{G}(t)\mathcal{P}\rho_0$ is the doorway prepared by the first two pulses, $\mathcal{G}(t)$ is its propagation and $\mathcal{W}(t)\equiv\hat{P}|\mathcal{G}(t)\mathcal{P}$ is the window for the signal; $\mathcal{P}\hat{A}=[\hat{P},\hat{A}]$ is the Liouville space polarization superoperator ($\hat{A}$ is an arbitrary operator) and $\mathcal{G}(t)\hat{A}=\theta(t)\exp(-i\hat{H}_M t)\hat{A}\exp(i\hat{H}_M t)$ is the Liouville space Green's function. $\theta(t)$ is the Heavyside step-function. Equation (10) is a different representation for eq. (4).

Invoking the rotating wave approximation (RWA) and expanding eq. (10) in the system eigenstates we can draw the Feynman diagrams shown in fig. 1c,d which represent the 2D PE signal with the initial density matrix $\rho(-\infty)\equiv|g\rangle\langle g|$. Equation (6) is represented by diagrams of fig. 1c which correspond to $\mathcal{G}_{e_4e_3,e_2e_1}(t_2)\propto\delta_{e_4e_2}\delta_{e_3e_1}$. The diagram in fig. 1d represents additional terms with $e_4=e_3$ and $e_2=e_1$ while $e_4\neq e_2$ corresponding to population relaxation. The response function is then

$$S^{(3)}=S^{(ESA)}+S^{(SE)}+S^{(GSB)}, \qquad (11)$$

where ESA, SE and GSB represent the excited state absorption (the third interaction corresponds to the absorption from the excited state e), stimulated emission (the third interaction corresponds to the induced emission from the excited state e) and ground-state bleaching (the third interaction corresponds to the ground-state absorption):

$$S^{(ESA)}=\sum_{fe_4e_3e_2e_1}\langle\mathcal{W}^{ll}_{fe_3}(t_3)\mathcal{G}_{e_4e_3,e_2e_1}(t_2)\mathcal{D}^{lr}_{ge_1}(t_1)\rangle, \quad (12)$$

$$S^{(SE)}=\sum_{e_4e_3e_2e_1}\langle\mathcal{W}^{lr}_{e_4g}(t_3)\mathcal{G}_{e_4e_3,e_2e_1}(t_2)\mathcal{D}^{lr}_{ge_1}(t_1)\rangle, \quad (13)$$

and

$$S^{(GSB)}=\sum_{e_2e_1}\langle\mathcal{W}^{ll}_{e_2g}(t_3)\mathcal{G}_{gg,gg}(t_2)\mathcal{D}^{rr}_{ge_1}(t_1)\rangle. \qquad (14)$$

The superscripts of the doorway and the window functions indicate interactions either on the left (ket) or on the right (bra) side of double-sided Feynman diagram. The subscripts indicate the density matrix elements and the angular brackets denote statistical averaging over bath fluctuations.

The Markovian approximation can be applied for fast bath modes, $Q^{(F)}$. During t_1 and t_3, $Q^{(F)}$ is responsible for homogeneous line broadening (diagonal fast fluctuations), while during t_2 it induces population relaxation and dephasing (off-diagonal fast fluctuations) described by a rate equation. In the secular approximation the Green's function is

$$\mathcal{G}_{e_4e_3,e_2e_1}(t_2)=\delta_{e_4e_2}\delta_{e_3e_1}e^{-(\gamma_{e_4}+\gamma_{e_3})t_2}+\delta_{e_4e_3}\delta_{e_2e_1}\tilde{\mathcal{G}}_{e_4e_2}(t_2), \qquad (15)$$

where $\tilde{\mathcal{G}}_{\nu\nu'}(\tau)$ is the probability of the bath-assisted transition from state ν' to state ν during τ and δ_{ab} is the Kronecker function. $\tilde{\mathcal{G}}$ satisfies the equation [19]

$$\frac{\mathrm{d}}{\mathrm{d}\tau}\tilde{\mathcal{G}}_{\nu\nu'}(\tau)=\sum_{\nu''}K_{\nu\nu''}\tilde{\mathcal{G}}_{\nu''\nu'}(\tau), \qquad (16)$$

where $K_{\nu\nu'}$ is the population transport rate matrix with the initial condition $\tilde{\mathcal{G}}_{\nu\nu'}(0)=\delta_{\nu\nu'}$.

Slow bath modes, $Q^{(S)}$, are responsible for spectral diffusion during t_1 and t_3. The diagonal parts of $Q^{(S)}$ induce shifts of system eigen energies, while the off diagonal parts can be eliminated by diagonalizing the system Hamiltonian together with $Q^{(S)}$ explicitely included. This is justified as long as the fluctuation amplitude is smaller than the energy gaps within one-exciton band and the timescale of $Q^{(S)}$ is longer than dephasing times γ^{-1}. We therefore apply the adiabatic approximation with respect to $Q^{(S)}$ and only retain diagonal slow fluctuations. Within this model eq. (16) still holds during t_2, but the rate matrix K is modulated by $Q^{(S)}$. In the case of smooth bath spectral density this modulation is of the order of $\bar{Q}^{(S)}/k_BT$, where $\bar{Q}^{(S)}$ is the modulation amplitude. When $\bar{Q}^{(S)}/k_BT\ll 1$, the modulation of transport rates can be neglected and $K(Q^{(S)})$ can be replaced by its mean $\bar{K}=\langle K(Q^{(S)})\rangle$, and $\tilde{\mathcal{G}}$ then does not depend on $Q^{(S)}$. The Green's function $\mathcal{G}(t)$ can then be factorized out in eqs. (12) and (13). We retain the dependence of interband coherences on $Q^{(S)}$ in t_1 and t_3 intervals in the doorway and window functions.

We shall calculate the transport contribution to the response function when populations change during t_2, by the cumulant expansion of eq. (11) with respect to the slow bath coordinate. New pathways not included in the coherent limit are presented by the diagram of fig. 1d. This diagram represents all contributions that depend on transport and will be used to describe SE and ESA of the photon echo by inverting wave vector directions.

The density matrix evolution in fig. 1d is described as follows. The first interaction occurs at time 0 on the left. During t_1 the system evolves in the electronic coherence ρ_{eg}. The second interaction (on the right) creates the population of the state e. During t_2 the population relaxes from ρ_{ee} to $\rho_{e'e'}$. During t_3 the system is again in an electronic coherence ρ_{bc}, where now b and c can be an arbitrary electronic states including the ground, e and f manifolds. The contribution of this diagram to the response function is

$$T(t_3,t_2,t_1)=-i^3\sum_{\nu e'e}\mu_{cb}\mu_{\nu e'}\mu^2_{eg}\tilde{\mathcal{G}}_{e'e}(t_2)\mathcal{F}^{(I)}_{cbe'e}(t_3,t_2,t_1), \qquad (17)$$

where $\nu \equiv b$ when the signal is generated on the left side of the diagram and $\nu \equiv c$ when it is generated on the right (here we used $\mu_{ab} = \mu_{ba}$). The dynamics of $\mathcal{F}^{(I)}$ comes solely from doorway and window funtions and invoking the Markovian approximation for $Q^{(F)}$ (superscript I denotes incoherent transport) we get:

$$\mathcal{F}^{(I)}_{cbe'e}(t_3,t_2,t_1) = e^{i\omega_{cb}\,t_3 - i\varepsilon_e t_1 - (\gamma_c+\gamma_b)t_3 - \gamma_e t_1} \times \langle e^{+i\hat{H}_c t_3} e^{-i\hat{H}_b t_3} e^{-i\hat{H}_g t_2} e^{-i\hat{H}_e t_1}\rangle, \quad (18)$$

where $\omega_{ab} = \varepsilon_a - \varepsilon_b$, γ_ν is the dephasing induced by $Q^{(F)}$ which is a sum of finite lifetime and pure dephasing: $\gamma_\nu = |K_{\nu\nu}|/2 + \bar{\gamma}_\nu$. $\hat{H}_\nu = \hat{Q}^{(S)}_{\nu\nu} + \hat{H}^{(S)}_B$ is the Hamiltonian of the excited state ν. We note that since fluctuations are defined with respect to the ground state, $Q_{gg} \equiv 0$. The ordering of the evolution operators for this pathway is defined using fig. 1d. Starting from the bottom-right we move anti-clockwise to c, then to b, and e.

We next expand all propagators with respect to $Q^{(S)}$ using state g as a reference and perform the cumulant expansion for $\mathcal{F}^{(I)}$. We finally get

$$\mathcal{F}^{(I)}_{cbe'e}(t_3,t_2,t_1) = \exp[i\omega_{cb}t_3 - i\varepsilon_e t_1 - (\gamma_c+\gamma_b)t_3 - \gamma_e t_1 + f^{(I)}_{cbe}(t_3,t_2,t_1)], \quad (19)$$

where

$$\begin{aligned} f^{(I)}_{cbe}(t_3,t_2,t_1) = {} & -g_{ee}(t_1) - g_{bb}(t_3) - g^*_{cc}(t_3) \\ & - g_{be}(t_1+t_2+t_3) + g_{be}(t_1+t_2) + g_{be}(t_2+t_3) \\ & + g_{ce}(t_1+t_2+t_3) - g_{ce}(t_1+t_2) - g_{ce}(t_2+t_3) \\ & + g_{cb}(t_3) + g^*_{bc}(t_3) + g_{ce}(t_2) - g_{be}(t_2). \end{aligned} \quad (20)$$

This expression contains lineshape functions coming from correlations during the time intervals t_1 and t_3.

The response function. – The complete response function for the photon echo consists of coherent (fig. 1c) and population transfer contributions (fig. 1d). The former are obtained by making the RWA to eq. (4). The latter are described by eq. (17). The response function depends on three ingredients $\mathcal{F}^{(C)}$, $\mathcal{F}^{(I)}$ and $\tilde{\mathcal{G}}$. The coherent part of populations must be multiplied by the probability of $e' = e$ during t_2, which is $\tilde{\mathcal{G}}_{ee}(t_2)$. Since coherences, $\rho_{\nu\nu'}$ with $(\nu \neq \nu')$, during t_2 do not mix with other density matrix elements we calculate their contributions using $\mathcal{F}^{(C)}$.

We shall partition the response function as

$$S^{(3)} = S^{(3)}_P + S^{(3)}_C, \quad (21)$$

where $S^{(3)}_P$ combines the terms with populations and $S^{(3)}_C$ with density matrix coherences during t_2. We then partition

$$S^{(3)}_l = S^{(ESA)}_l + S^{(SE)}_l + S^{(GSB)}_l;\ l = P, C, \quad (22)$$

where

$$\begin{aligned} S^{(ESA)}_P(t_3,t_2,t_1) = {} & i\sum_{ee'}\sum_f \mu^2_{fe'}\mu^2_{ge}\tilde{\mathcal{G}}_{e'e}(t_2) \\ & \times [\delta_{ee'}\mathcal{F}^{(C)*}_{efe}(t_1, t_1+t_2, t_1+t_2+t_3, 0) \\ & + \zeta_{ee'}\mathcal{F}^{(I)*}_{fe'e'e}(t_3,t_2,t_1)], \end{aligned} \quad (23)$$

$$\begin{aligned} S^{(SE)}_P(t_3,t_2,t_1) = {} & -i\sum_{ee'}\mu^2_{ge}\mu^2_{ge'}\tilde{\mathcal{G}}_{e'e}(t_2) \\ & \times [\delta_{ee'}\mathcal{F}^{(C)}_{ege}(0, t_1+t_2, t_1+t_2+t_3, t_1) \\ & + \zeta_{ee'}\mathcal{F}^{(I)*}_{e'ge'e}(t_3,t_2,t_1)], \end{aligned} \quad (24)$$

$$\begin{aligned} S^{(GSB)}_P(t_3,t_2,t_1) = {} & -i\sum_{ee'}\mu^2_{ge'}\mu^2_{ge} \\ & \times \mathcal{F}^{(C)}_{ege'}(0, t_1, t_1+t_2+t_3, t_1+t_2), \end{aligned} \quad (25)$$

and

$$\begin{aligned} S^{(ESA)}_C(t_3,t_2,t_1) = {} & i\sum_{e\neq e'}\sum_f \mu_{fe'}\mu_{fe}\mu_{ge'}\mu_{ge} \\ & \times \mathcal{F}^{(C)*}_{e'fe}(t_1, t_1+t_2, t_1+t_2+t_3, 0), \end{aligned} \quad (26)$$

$$\begin{aligned} S^{(SE)}_C(t_3,t_2,t_1) = {} & -i\sum_{e\neq e'}\mu^2_{ge}\mu^2_{ge'} \\ & \times \mathcal{F}^{(C)}_{ege'}(0, t_1+t_2, t_1+t_2+t_3, t_1), \end{aligned} \quad (27)$$

with $S^{(GSB)}_C \equiv 0$. Here $\zeta_{ab} \equiv 1 - \delta_{ab}$. At $t_2 = 0$ exciton transfer has not occured yet, and fluctuations contribute only through dephasing. At long t_2 only populations during t_2 survive, then the response is given by S_P.

Fluctuation model with Stokes shift. – In this section we use a more restricted model for fluctuations by assuming a single collective coordinate $\hat{Q}^{(S)}$ coupled to all exciton states during t_2. We thus neglect slow intraband energy fluctuations. In this case all one-exciton states are correlated and bath evolution does not depend explicitely on the state index. For this model we can include excited state evolution with $Q^{(S)}$ during t_2 and hence the bath reorganization (dynamic Stokes shift). We will thus assume that the bath in the excited state during t_2 evolves in state e'. By making the Markovian approximation with respect to the $Q^{(F)}$ in eq. (17) we obtain

$$\mathcal{F}^{(I)}_{cbe'e}(t_3,t_2,t_1) = e^{i\omega_{cb}t_3 - i\varepsilon_e t_1 - (\gamma_c+\gamma_b)t_3 - \gamma_e t_1} \times \langle e^{+i\hat{H}_{e'}t_2} e^{+i\hat{H}_c t_3} e^{-i\hat{H}_b t_3} e^{-i\hat{H}_{e'}t_2} e^{-i\hat{H}_e t_1}\rangle. \quad (28)$$

Due to transport e' varies during t_2, however $Q^{(S)}$ remains the same (since evolution during t_2 on the right side of diagram is in the excited state, we need to include it explicitely, which we skipped in eq. (18)). The cumulant expansion for $\mathcal{F}^{(I)}$ then gives

$$\mathcal{F}^{(I)}_{cbe'e}(t_3,t_2,t_1) = \exp[i\omega_{cb}t_3 - i\varepsilon_e t_1 - (\gamma_c+\gamma_b)t_3 - \gamma_e t_1 + f^{(I)}_{cbe(e')}(t_3,t_2,t_1)], \quad (29)$$

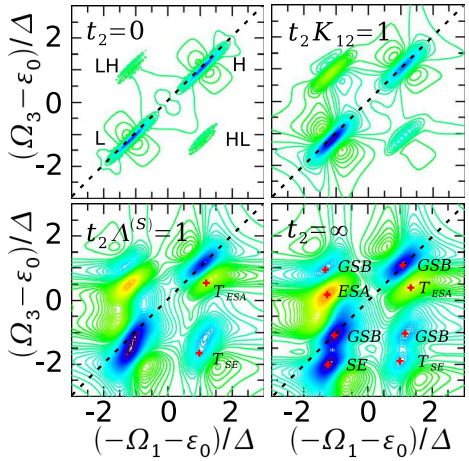

Fig. 2: (Color online) 2D PE signal ($\mathrm{Im}S^{(3)}(\Omega_3,t_2,\Omega_1)$) of a dimer at different t_2 delays; the model parameters are given in fig. 3. Equations (22)–(27) using eq. (8) and eq. (30) were used to calculate the signals. Contributions from ESA, SE and GSB are clearly marked on the 2D plot.

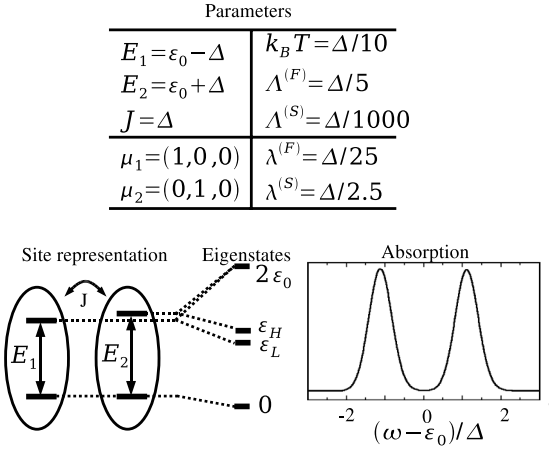

Fig. 3: Scheme, parameters and absorption of the model dimer. Relations between parameters are $k_BT \ll \Delta$, $\Lambda^{(F)2}/(\lambda^{(F)}k_BT) \gg 1$ (fast limit), $\Lambda^{(S)2}/(\lambda^{(S)}k_BT) \ll 1$ (slow limit), inhomogeneous linewidth $\gamma_i = \sqrt{\lambda^{(S)}k_BT} < \Delta$, homogeneous linewidth $\gamma_h = \lambda^{(F)}k_BT/\Lambda^{(F)} < \gamma_i$ and $\Lambda^{(S)} < K$ (population transport rate from higher-energy single-exciton state to the lower-energy state —rate in the opposite direction is not included). $\Lambda^{(F)}$ induces uncorrelated fluctuations of site transition energies, while slow fluctuations are completely correlated.

where

$$f^{(I)}_{cbe'e}(t_3,t_2,t_1) = f^{(I)}_{cbe}(t_3,t_2,t_1) + 2i\,\mathrm{Im}[g_{ce'}(t_2+t_3) - g_{ce'}(t_2) - g_{ce'}(t_3) + g_{be'}(t_2) - g_{be'}(t_2+t_3) + g_{be'}(t_3)], \quad (30)$$

where Im denotes the imaginary part. The expression now has the same limit for $t_2 \to \infty$ as in ref. [4] when bath correlations completely decay.

Application to a model dimer. – We demonstrate our results for a model system of two coupled two-level molecules. We assume that the two transitions are well separated and do not spectrally overlap. The transition energy of each chromophore $j=1,2$ is $E_j = \varepsilon_0 \pm \Delta$, where Δ is the detuning parameter. The coupling between chromophores is J. The eigenenergies of the system we denote ε_L (lower energy), ε_H (higher-energy singly excited state) and $2\varepsilon_0$ (doubly excited state).

The bath is represented by two overdamped Brownian oscillator coordinates inducing site energy fluctuations $\tilde{E}_j(t)$ with correlation decay rates $\Lambda^{(F)}$ (fast) and $\Lambda^{(S)}$ (slow). $\Lambda^{(F)}$ induces uncorrelated fluctuations while $\Lambda^{(S)}$ creates fully correlated fluctuations. The correlation function of site energy fluctuations $C_{jj'}(t) \equiv \langle \tilde{E}_j(t)\tilde{E}_{j'}(0)\rangle = \delta_{jj'}C^{(F)}(t) + C^{(S)}(t)$, where $C^{(l)}(t)$ $(l=S,F)$ is the site energy correlation function.

We model the spectral density of local chromophore energy fluctuations as $C^{(l)}(\omega) = 2\lambda_l\omega\Lambda_l(\omega^2+\Lambda_l^2)^{-1}$ giving the effective lineshape function

$$g^{(l)}(t) = \lambda^{(l)}\Lambda^{(l)-2}(2k_BT - i\Lambda^{(l)})(e^{-\Lambda^{(l)}t} + \Lambda^{(l)}t - 1), \quad (31)$$

where T is the temperature and k_B is the Boltzmann constant.

The transformation of this model to the eigenbasis is given in [4]. Population transport rates were calculated using equation (C3) of [25].

The 2D PE for various delay times t_2 calculated using eqs. (22)–(27) using eq. (8) and eq. (30) are shown in fig. 2 (the model parameters are given in fig. 3). The signal at $t_2=0$ consists of four regions: two diagonal peaks (L, lower energy and H, higher energy; the diagonal is shown by a dashed line) and two crosspeak regions LH and HL. The diagonal peaks are elongated diagonally due to $\Lambda^{(S)}$: the widths across and along the diagonal represent homogeneous and inhomogeneous linewidths, respectively. These peaks consist of GSB (with $e=e'$ in fig. 1c) and SE ($e=e'$) contributions; both are negative (blue online). The crosspeaks are also elongated in the same direction due to positive correlations. GSB ($e \neq e'$) —negative, SE ($e \neq e'$) —negative and ESA —positive contribute in this region.

At $t_2 = K_{12}^{-1}$, population partially transfers to the L state and the SE contribution of the L peak increases at the same time increasing the ESA contribution in the LH region (yellow online) while the ESA in the HL region originating from the H state decays (blue online —GSB survives). All peaks become broader in the anti-diagonal direction due to the loss of correlations of the slow coordinate.

Additional contributions of SE and ESA appear along $\Omega_1 = -\varepsilon_H$ due to exciton transfer from H to L. They are induced by the diagram of fig. 1d and become well resolved at $t_2\Lambda^{(S)} = 1$ where all $e \neq e'$ contributions disappear since $\Lambda^{(S)} \ll K_{12}$ and Stokes shift become visible as correlations

decay. The ESA contribution from exciton transfer is marked as T_{ESA} (positive) and SE contribution is marked T_{SE} (negative). They separate from H and HL compared to $t_2 = 0$ due to Stokes shift formation.

At long t_2 the bath correlations of $\Lambda^{(S)}$ disappear and thus all peaks become broad anti-diagonal and the Stokes shift of diagonal and off-diagonal peaks become intense.

Discussion. – We have calculated the 2D PE signal by incorporating statistical properties of fluctuating bath coordinates and population relaxation. Our expressions rely on the separation of bath timescales —approximation that is commonly used by describing optical properties. In absorption spectra the fast bath modes are responsible for homogeneous linewidth, while slow modes lead to inhomogeneous linewidth (static limit). The photon echo techniques can estimate homogeneous linewidth and population relaxation and additionally probe the decay of fluctuation correlations. The static limit then does not apply and extension to the finite regime is provided by our theory. Most of the present simulations assume fast bath modes and simulate static disorder numerically. We extended the expressions to the regime of fast and slow timescales which show up as dynamics of peak lineshapes in 2D PE spectra. Therefore we can describe population relaxation and decay of correlations at early t_2 times. When the fluctuation and population relaxation timescales are comparable the signal can be calculated by numerical simulation of the quantum dynamics [17].

Equations (20) and (30) represent two levels of theory: eq. (20) holds for arbitrary bath fluctuations when the *inhomogeneous linewidth* $< k_B T$, while eq. (30) describes arbitary inhomogeneous linewidth but for correlated slow energy fluctuations. In the former case the Stokes shift is small, while in the latter the shift is properly incorporated. The Stokes shift should be relevant to photosynthetic systems where large-scale protein motions induce correlated fluctuations. In vibrational spectroscopy the linewidth is usually smaller than $k_B T$ and the Stokes shifts are negligible. In both cases bath correlations are preserved for $t_2 \Lambda^{(S)} < 1$. The interplay of transport dynamics and correlation decays will be visible when $\Lambda^{(S)}$ is comparable to K. In 2D PE, finite bath timescales are responsible for time evolving lineshapes as bath correlations decay with t_2. Exciton transport and bath correlations on this timescale are observed in photosynthetic systems [6] and vibrations of peptides [9]. We have assumed overdamped bath model. Correlated fluctuation dynamics due to underdamped bath modes has been recently observed [7].

The present application was made to a model dimer system, which is the simplest excitonic aggregate. However, our obtained expressions are not limited to dimeric systems and can describe correlated dynamics in arbitrary multilevel excitonic systems.

* * *

This research was supported by the National Science Foundation grant No: CHE-0446555 and the National Institutes of Health GM59230. LK is grateful for the financial support from the Lithuanian State Science and Studies Foundation.

REFERENCES

[1] Tanimura Y. and Mukamel S., *J. Chem. Phys.*, **99** (1993) 9496.
[2] Mukamel S., *Annu. Rev. Phys. Chem.*, **51** (2000) 691.
[3] Wright J. C., *Int. Rev. Phys. Chem.*, **21** (2002) 185.
[4] Zhang W. M., Meier T., Chernyak V. and Mukamel S., *J. Chem. Phys.*, **108** (1998) 7763.
[5] Prall B. S., Parkinson D. Y. and Fleming G. R., *J. Chem. Phys.*, **123** (2005) 054515.
[6] Brixner T., Stenger J., Vaswani H. M., Cho M., Blankenship R. E. and Fleming G. R., *Nature*, **434** (2005) 625.
[7] Engel G. S., Calhoun T. R., Read E. L., Ahn T. K., Mančal T., Cheng Y. C., Blankenship R. E. and Fleming G. R., *Nature*, **446** (2007) 782.
[8] Chung H., Khalil M., Smith A. W., Ganim Z. and Tokmakoff A., *Proc. Natl. Acad. Sci. U.S.A.*, **102** (2005) 612.
[9] Demirdöven N., Khalil M. and Tokmakoff A., *Phys. Rev. Lett.*, **89** (2002) 237401.
[10] Fang C., Wang J., Kim Y. S., Charnley A. K., Barber-Armstrong W., Smith A. B. III, Decatur S. M. and Hochstrasser R. M., *J. Phys. Chem. B*, **108** (2004) 10415.
[11] Mukamel S. and Abramavicius D., *Chem. Rev.*, **104** (2004) 2073.
[12] Zhuang W., Abramavicius D. and Mukamel S., *Proc. Natl. Acad. Sci. U.S.A.*, **102** (2005) 7443.
[13] Kolano C., Helbing J., Kozinski M., Sander W. and Hamm P., *Nature*, **444** (2006) 469.
[14] Fecko C. J., Eaves J. D., Loparo J. J., Tokmakoff A. and Geissler P. L., *Science*, **301** (2003) 1698.
[15] Mukamel S., *Principles of Nonlinear Optical Spectrscopy* (Oxford University Press, New York) 1995.
[16] Cho M., Scherer N. F., Fleming G. R. and Mukamel S., *J. Chem. Phys.*, **96** (1992) 5618.
[17] Gelin M. F., Egorova D. and Domcke W., *J. Chem. Phys.*, **123** (2005) 164112.
[18] Mukamel S., *Phys. Rev. A*, **28** (1983) 3480.
[19] Tanimura Y., *J. Phys. Soc. Jpn.*, **75** (2006) 082001.
[20] Jansen T. C., Hayashi T., Zhuang W. and Mukamel S., *J. Chem. Phys.*, **123** (2005) 114504.
[21] Šanda F. and Mukamel S., *J. Chem. Phys.*, **125** (2006) 014507.
[22] Brixner T., Mančal T., Stiopkin I. V. and Fleming G. R., *J. Chem. Phys.*, **121** (2004) 4221.
[23] Kjellberg P., Brüggemann B. and Pullerits T., *Phys. Rev. B*, **74** (2006) 024303.
[24] Chernyak V. and Mukamel S., *J. Chem. Phys.*, **105** (1996) 4565.
[25] Chernyak V., Minami T. and Mukamel S., *J. Chem. Phys.*, **112** (2000) 7953.